Supplementary Information

Anomalous lattice anharmonicity and spin-lattice coupling in spin-orbit coupled halide K_2IrBr_6

Smriti Bhatia,[a] Arshid Ahmad [a,b], Mohd Zeeshan,[a] Simranjeet Kaur,[a] Reshma Kumawat[a], Shubham Farswan[a], Jay Krishna Anand,[c], Ankur Goswami,[c] Brajesh K Mani,[a] Kaushik Sen,*[a]

[a]Department of Physics, Indian Institute of Technology Delhi, Hauz Khas, New Delhi 110016, India
[b]Institute of Condensed Matter Physics, Technische Universität Darmstadt, 64289 Darmstadt, Germany
[c]Department of Materials Science and Engineering, Indian Institute of Technology Delhi, Hauz Khas, New Delhi-110016, India

Distortions in KIB:

Fig. S 1 summarizes various structural distortions in K_2IrBr_6 as reported by N. Khan et al.[1] KIB is cubic (α) at room temperature, becomes tetragonal (β) below ≈170 K, and then monoclinic (γ) below ≈122 K. The symmetry-lowering is dominated by cooperative rotations (φ), which correspond to in-plane rotations of the $IrBr_6$ octahedra. At lower T, this is accompanied by: cooperative deformations (δ_t and δ_0), tetragonal strain (η) and tilts (ψ) of the $IrBr_6$ octahedra. The tetragonal deformation δ_t is gauged by $\delta_t = (d_2 - d_1)/(d_2 + d_1)$, where d_1 and d_2 are the in-plane and out-of-plane distances in the $IrBr_6$ octahedra. The orthorhombic deformation δ_0 is defined as $\delta_0 = (d_1 - d_1^{'})/(d_1 + d_1^{'})$, where d_1 and $d_1^{'}$ are the in-plane distances in the $IrBr_6$ octahedra.

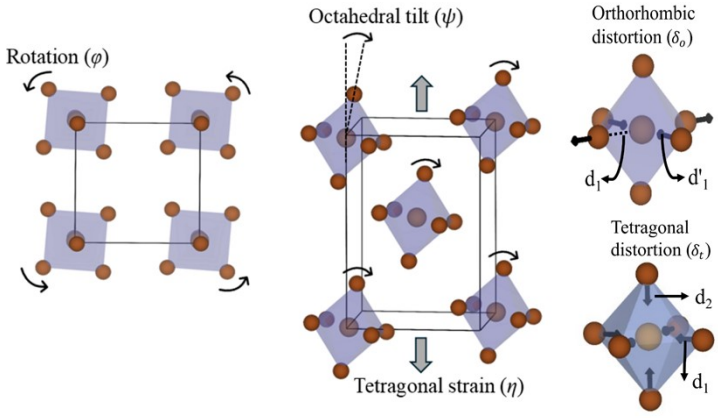

Fig. S 1 Distortions of the K_2IrBr_6 structure. Octahedral rotation ( ) and tilt ( ) of the $IrBr_6$ octahedra. Tetragonal ( ) and orthorhombic ( ) deformations of the octahedra, as well as tetragonal strain ( ). This figure is adapted from Khan et al.[1]

Raman active phonon modes in tetragonal and monoclinic phases:

Table S 1. and Table S 2. lists the phonon mode energies for the tetragonal and monoclinic phases, respectively.

Table S 1. Fourteen Raman Active modes at zone-center for tetragonal phase at zone-center (Γ point).

Γ_{Raman}	ω_{cal} (cm^{-1})	Γ_{Raman}	ω_{cal} (cm^{-1})
A_{1g}	----	B_{2g}	110.78
E_g	----	E_g	111.28
E_g	37.99	B_{1g}	112.32
E_g	59.23	B_{1g}	189.09
B_{1g}	68.03	B_{2g}	189.49
E_g	73.20	A_{1g}	190.79
E_g	99.04	A_{1g}	222.67

Table S 2. Twenty-four Raman Active modes at zone-center for Monoclinic phase at the zone-center (Γ point).

Γ_{Raman}	ω_{cal} (cm^{-1})	Γ_{Raman}	ω_{cal} (cm^{-1})	Γ_{Raman}	ω_{cal} (cm^{-1})
B_g	----	A_g	75.37	B_g	126.26
A_g	----	B_g	75.70	A_g	126.96
B_g	9.34	A_g	85.30	A_g	179.22
A_g	21.67	B_g	95.81	B_g	180.62
A_g	35.51	A_g	98.25	A_g	193.96
B_g	43.02	B_g	106.38	B_g	198.36
B_g	61.53	B_g	111.02	B_g	221.11
A_g	64.53	A_g	117.05	A_g	225.55

Full set of EPR spectra and corresponding Fit Parameters:

Fig. S 2 Derivative EPR spectra of polycrystalline KIB. displays the derivative EPR spectra of KIB spanning a temperature range from 100 K to 300 K. The extracted fit parameters for EPR spectra of KIB, including the resonance field ($\mu_0 H_r(Oe)$), and corresponding fitting uncertainties are summarized in Table S 3.

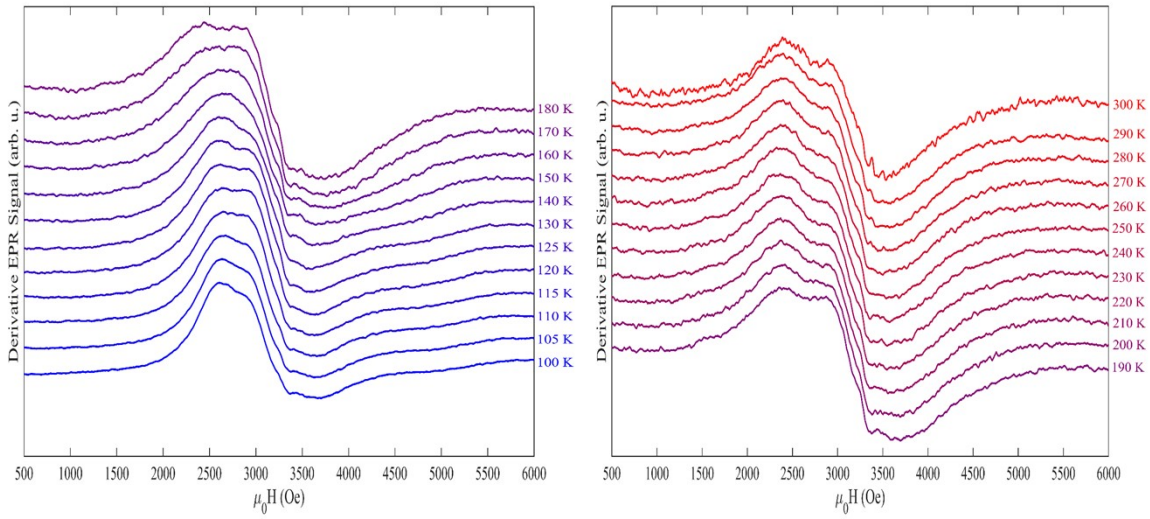

Fig. S 2 Derivative EPR spectra of polycrystalline KIB.

Table S 3. Best-fit resonance field ($^{\mu_0 H_r(Oe)}$) values and corresponding standard errors obtained from the fitting of EPR spectra of KIB.

T (K)	Mode 1 ($\mu_0 H_r(Oe)$)	Error (±)	Mode 2 ($\mu_0 H_r(Oe)$)	Error (±)	Mode 3 ($\mu_0 H_r(Oe)$)	Error (±)	Mode 4 ($\mu_0 H_r(Oe)$)	Error (±)
300	2563.61	16.175	3143.96	17.397	3785.38	53.887	----	----
290	2577.97	20.423	3137.96	41.516	3579.49	152.940	----	----
280	2576.72	21.972	3132.53	38.842	3620.61	137.970	----	----
270	2571.98	20.021	3125.74	39.940	3571.18	163.889	----	----
260	2579.95	18.626	3134.09	32.625	3664.81	128.296	----	----
250	2581.73	23.871	3129.16	41.602	3588.78	144.585	----	----
240	2586.72	26.036	3132.38	43.515	3588.13	159.548	----	----
230	2585.48	18.850	3131.27	24.145	3620.28	66.404	----	----
220	2579.48	18.373	3136.39	3.560	3630.11	32.168	----	----
210	2580.21	22.455	3141.54	28.817	3637.63	92.630	----	----
200	2572.58	22.086	3139.81	29.130	3647.89	91.402	----	----
190	2557.41	26.489	3127.36	31.100	3599.85	95.590	----	----
180	2557.14	30.726	3116.05	31.422	3594.01	90.040	----	----
170	2576.51	50.642	3112.19	35.735	3606.62	122.066	----	----
160	2622.87	60.452	3109.78	42.524	3596.60	157.752	----	----
150	2743.71	39.369	3160.67	76.193	3436.42	106.583	4548.58	44.025
140	2751.38	27.368	3157.25	87.937	3335.01	142.079	4589.59	46.809
130	2716.54	18.393	3148.25	59.151	3326.80	112.235	4742.71	38.151
125	2701.65	14.443	3140.38	49.301	3298.44	103.523	4803.53	34.015
120	2698.26	16.880	3101.31	87.978	3205.09	144.097	4822.55	34.286
115	2715.81	18.521	3080.80	81.823	3178.21	114.217	4887.49	28.624
110	2720.54	16.709	3058.77	70.642	3166.75	86.820	4894.35	28.691
105	2710.67	11.677	3046.15	48.914	3169.36	61.518	4883.82	22.929
100	2699.14	10.604	3030.16	46.043	3156.62	56.467	4826.61	25.067

EPR Reproducibility:

Fig. S 3 Comparison of EPR spectra of KIB recorded at (a) 100 K, (b) 120 K, and (c) 150 K from two different batches of KIB measured over a period of 5 months. compares the derivative EPR spectra (dP/dH) of KIB obtained from two independent measurements taken five months apart at selected temperatures (100 K, 120 K, 150 K). Since EPR spectra are recorded as first-derivative signals, small variations in baseline, modulation amplitude, or signal-to-noise ratio can significantly affect the apparent line shape, making exact spectrum-to-spectrum reproducibility challenging. However, consistent measurements are maintained across varying temperatures over a period of five months on two distinct batches of KIB.

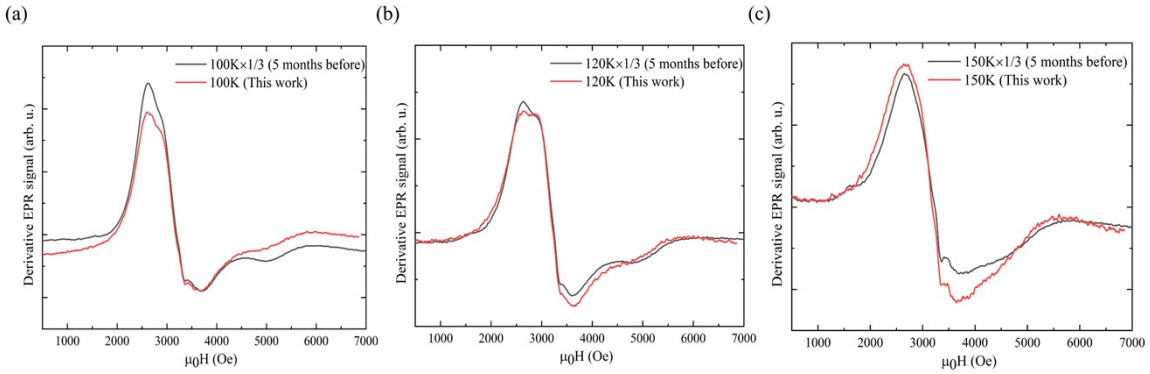

Fig. S 3 Comparison of EPR spectra of KIB recorded at (a) 100 K, (b) 120 K, and (c) 150 K from two different batches of KIB measured over a period of 5 months.

References:

1 N. Khan, D. Prishchenko, M. H. Upton, V. G. Mazurenko and A. A. Tsirlin, *Phys. Rev. B*, 2021, **103**, 125158.